Modelling the Effect of Grooved Barrels on the Performance of Single Screw Extruders

A Gaspar-Cunha, José A. Covas, Janusz Sikora

Abstract

Single screw extruders containing grooved barrels are used in many industrial extrusion lines, for example to manufacture plastics pipes and blown film. Through an increase of the drag friction forces between the polymer and the barrel, the conveying capacity of the screw is enhanced, yielding higher outputs and better process stability. This chapter presents and assesses computationally models for considering the effect of the presence of longitudinal or helical grooves near to the inlet port of the barrel of single screw extruders. The results obtained demonstrate that the existence of grooves clearly improves the performance of the extruder.

1- Introduction

The underlying mechanism of solids conveying along the channel of a single screw extruder is well established [1-3]. Assuming that the solids form a cohesive plug maintaining good contact with the surrounding metallic surfaces (i.e., inner barrel wall, screw root, and pushing and trailing flights), the effect of the friction coefficients between the solids and the barrel, f_b, and between the solids and the screw, f_s, must be considered. Their relative magnitude will influence the corresponding dragging forces and, consequently, the displacement of the plug along the barrel. If $f_s > f_b$, the polymer will stick to the screw and slip on the barrel. Thus, the material will not move forward and the output is nil. Contrarily, if $f_b > f_s$, the material slips on the screw, progressing axially. This explains why, in practice, the surface of the screw channel is polished, while that of the barrel is kept relatively rough. The higher the difference between the friction coefficients, the higher the output. This prompted the concept of a grooved barrel near to the entry port of the extruder: if $f_b >> f_s$, not only the output is high, but it is also more stable [3], i.e., less dependent on fluctuations in melting, melt viscosity and die resistance. During the 1960's the concept found practical application in Germany, and progressively extended to european equipment manufacturers, especially for the extrusion of pipes and blown-film. Due to the popularity achieved, conventional extruders became known as "smooth bore extruders" in contrast with "grooved feed extruders".

Groove-feed extruders are still not very popular in the U.S.A., probably because they also have a number of disadvantages/requisites:

- The grooves should be relatively short (generally, lesser than 5D), in order to limit the pressure generated (which increases exponentially downstream) - this can reach 100 - 300 MPa; also, abrasion and mechanically resistant materials should be used for machining screw and barrel;
- Conversely, the friction forces generated will dissipate heat and could induce premature melting of the material, i.e., insufficient pressure generation; thus, it is important to assure the capacity of cooling the grooves via a circulating fluid and the existence of a thermal barrier with the remaining of the barrel;
- Higher friction forces require more torque for the same screw speed, i.e., a more powerful motor and a higher energy consumption;
- Screws with small compression ratio are usually mandatory, in order to limit the pressure generated; however, these screws have lower melting efficiency;
- The performance of the grooves is very sensitive to the characteristics of the solids; generally, they are not suitable to processing soft pellets (such as those of thermoplastic elastomers), powders and regrinds, due to possible plugging;
- The presence/flow of pellets in the grooves may affect the self-cleaning time of the extruder.

Due to the practical importance of the topic, numerous theoretical and experimental studies have been performed during the last forty years on groove feed extruders [3-11]. Two major modelling approaches have been developed, one assuming a global coefficient of friction resulting from the geometry of the grooves, while the other considers contribution of the flow of pellets inside the grooves. Due to the possibility of using analytical solutions, this chapter adopts the first approach. Four models proposed in the open literature are assessed in terms of their suitability and their sensitivity to changes in geometric parameters. Finally, the effect of the geometry of the grooves on the performance of a laboratorial extruder will be studied, with the aim of generating data that later could be compared with values obtained experimentally.

2- Geometry of the grooves

Grooves can be longitudinal or helical, as illustrated schematically in Figure 1. They are generally distributed evenly around the perimeter of the inner barrel wall. The cross-section can be rectangular, semi-circular, semi-drop shaped, or saw-toothed, but the former seems to be the most popular due its simpler machining. Usually, the depth of the grooves (h_N) decreases gradually from a maximum value at the entrance (h_{N0}) to zero at the outlet:

$$h_N = h_{N0} - A\, Z_N \quad \textbf{(1)}$$

where A is the slope and Z_N is the length. This solution minimizes the probability of the pellets being retained in the grooves. While longitudinal grooves create a higher global friction coefficient, the helical solution induces the same effect, and the helix angle creates a positive drag component for the material inside the grooves.

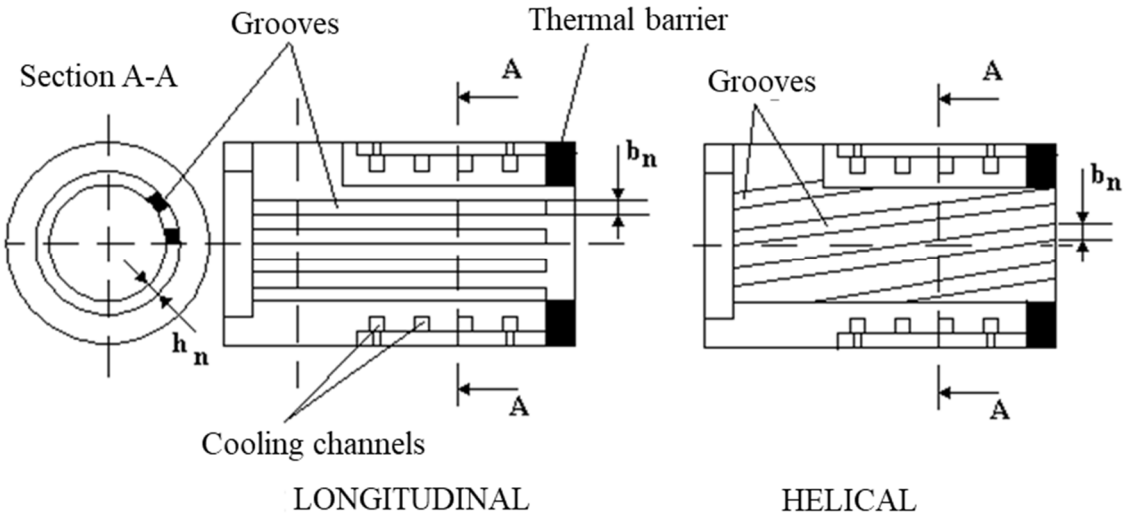

Figure 1- Longitudinal and helical grooves in the barrel.

3- Models assuming a global friction coefficient in the grooves

This approach assumes that the friction coefficient for a smooth bore extruder, f_b, can be replaced by a larger global, or equivalent, friction coefficient in the presence of grooves, f_{ef}. As shown in Figure 2, in the presence of grooves, three friction coefficients play a role in the transport of the solids: polymer-barrel, f_b, polymer-screw, f_s, and polymer-polymer, $f_{p\text{-}p}$. Therefore, this approach ignores the dynamics of flow in the grooves.

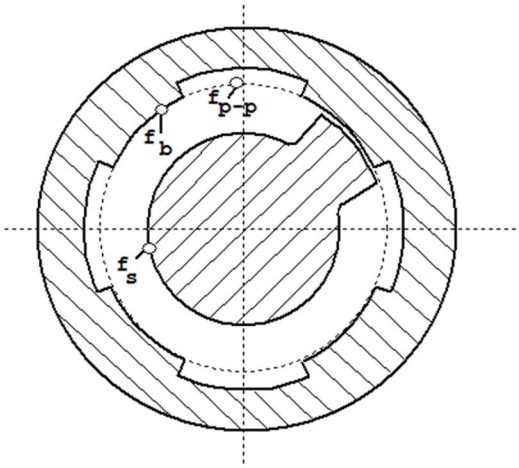

Figure 2- Friction coefficients in the presence of grooves

Goldacker [11] proposed an equation for f_{ef} that contains the contribution of f_b and f_{p-p}:

$$f_{ef} = f_b + \left(f_{p-p} - f_b\right)\frac{B}{\pi D_b} \quad \textbf{(2)}$$

where D_b is the internal diameter of the barrel and B is the total grooves width, given by:

$$B = b_N N_N \quad \textbf{(3)}$$

This method does not consider the number of grooves nor their depth, whose influence has been shown as considerable [6, 8]. To overcome this, Potente [5] proposes the following equation:

$$f_{ef} = f_b + \left(f_{p-p} - f_b\right)\frac{B}{\pi D_b}\left\{1 - \exp\left[-\alpha\left(\frac{h_N}{B} N_N\right)^{\beta}\right]\right\} \quad \textbf{(4)}$$

α and β are empirical constants that are approximately equal to 5 and 0.9, respectively [5]. If the coefficients of friction in the inner surface of the barrel, f_b, and at the base of the grooves, f_{Na}), are different ($f_{Na} \geq f_b$>), the equation becomes:

$$f_{ef} = \left[f_b + \left(f_{p-p} - f_b\right)\frac{B}{\pi D_b}\right]\left\{1 - \exp\left[-0.65\left(\frac{f_{Na}}{f_b} - 1\right)^{1.2}\right]\right\} + \quad \textbf{(5)}$$

$$\left[f_b + \left(f_{p-p} - f_b\right)\frac{B}{\pi D_b}\left\{1 - \exp\left[-5\left(\frac{h_N}{B} N_N\right)^{9}\right]\right\}\right]\exp\left[-0.65\left(\frac{f_{Na}}{f_b} - 1\right)^{1.2}\right]$$

Rautenbach and Peiffer [6, 7] performed force balances for an element of the solid plug in the channel and assumed the validity of the Hooke's Law. Neglecting the effects of inertia and gravity, as well as the distribution of transverse stresses in the downchannel direction, for the coordinate system shown in Figure 3, they obtained the following expression for a balance of the friction forces acting on the grooves:

$$f_{ef} = \frac{1}{e^{A^+\varphi_E} - 1} \sum_{n=1}^{M} \left\{ f_b \left[e^{A^+(n\varphi_F + (n-1)\varphi_N)} - e^{A^+(n-1)(\varphi_N + \varphi F)} \right] + f_{p-p} \left[e^{A^+ n(\varphi_N + \varphi F)} - e^{A^+(n\varphi_F + (n-1)\varphi_N)} \right] \right\} \quad \textbf{(6)}$$

where:

$$M = \frac{\varphi_E}{\varphi_F + \varphi_N} \quad \textbf{(7)}$$

φ_E is the adimensional screw channel length:

$$\varphi_E = 2\pi E \cos\theta_b \quad \textbf{(8)}$$

φ_N is the angle shown in Figure 3:

$$\varphi_N = arctg \frac{b_N}{D_B} \quad \textbf{(9)}$$

φ_F is the angle shown in Figure 3:

$$\varphi_F = \frac{2\pi - N_N \varphi_N}{N_N} \quad \textbf{(10)}$$

A^+ is ~ 0.5, E is the number of screw turns facing grooves and θ_b is the screw helix angle.

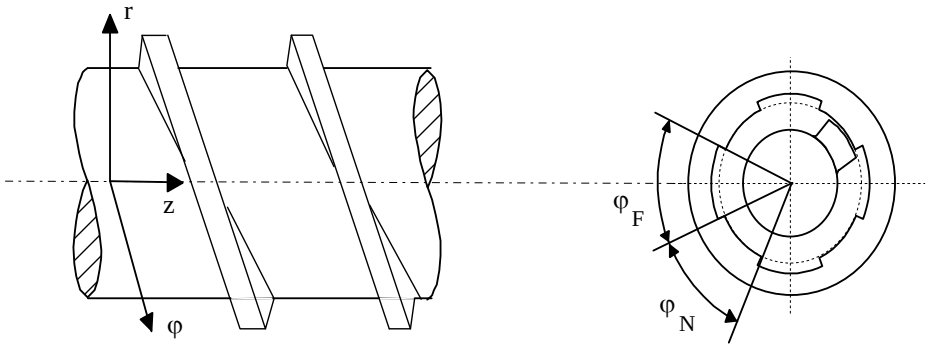

Figure 3- System of coordinates and geometrical parameters for the model proposed by Rautenbach and Peiffer [6, 7].

Grünschloβ [8] considered the presence of transverse flow of polymer granules in the grooves (see Figures 4 and 5). He observed that the latter becomes significant when the ratio h_N/b_N is small (Figure 5). Thus, two situations may occur:

- If h_N/b_N is greater than a critical value, the average friction coefficient is obtained from equation 2;

- Otherwise, its value varies between the value given by equation 2 and f_b (Figure 6); in this case, higher pressures develop along the grooves.

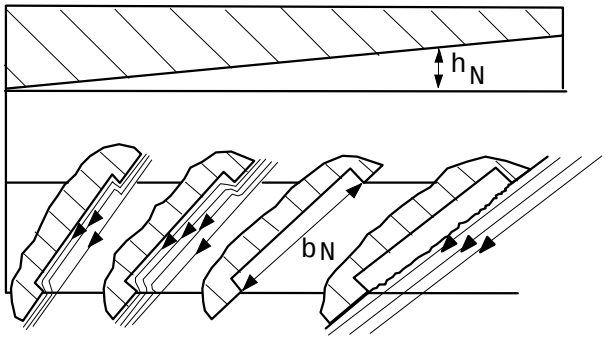

Figure 4 - Transverse flow of polymer granules in the grooves.

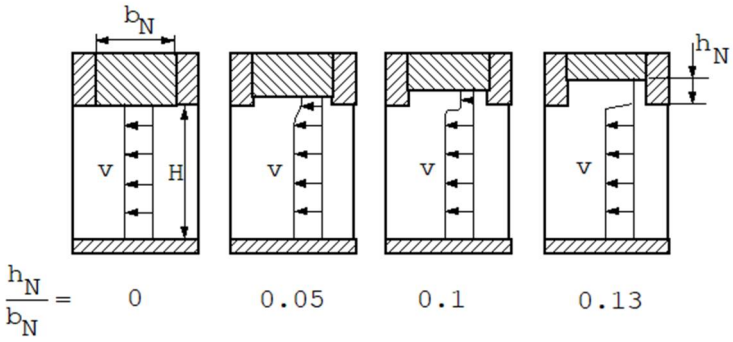

Figure 5 - Velocity profiles in the screw channel and transversal to the grooves.

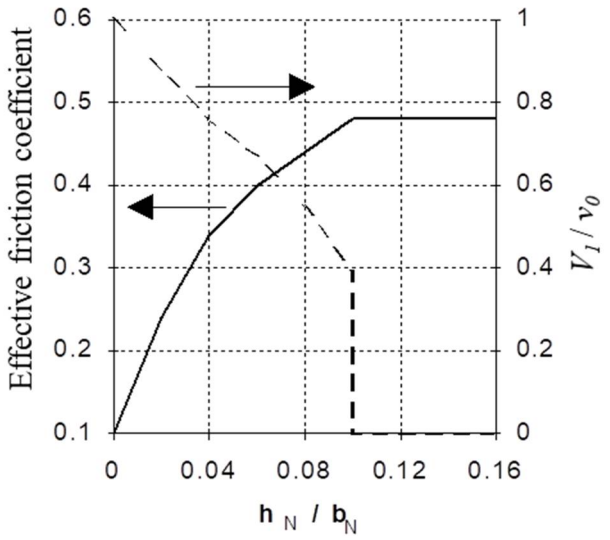

Figure 6 - Coefficient of friction and velocity of the solid bed as a function of h_N/b_N (f_b = 0.11 and f_{p_p} = 0.48).

These observations were used to build the model represented in Figure 7. The model assumes that the total power consumed to maintain the flow naturally adjusts to a minimum value ($P_{Ges\ min}$).

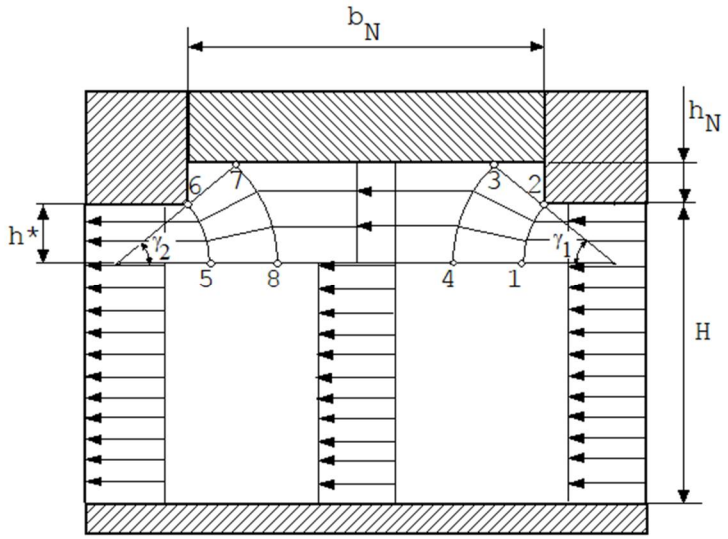

Figure 7 - Model illustrating the transversal flow in the grooves.

The total power (P_{Ges}) is due to the deformations in zones 1 to 4 and 5 to 8, the deflections in zones 1-2, 3-4, 5-6 and 7-8 and the friction at zones 1-4, 5-8, 2-3, 6-7, 3-7, and 4-8:

$$P_{Ges} = 4P_{1-2} + 2P_{1-2-3-4} + 2P_{1-4} + 2P_{2-3} + P_{3-7} + P_{4-8} \quad \textbf{(15)}$$

Where P_i represents a dimensionless power consumption. These values depend on γ_1, γ_2 and h^*, and can be obtained from the following equations, for $\gamma_1 = \gamma_2 = \gamma$:

$$P_{1-2} = \frac{h^*}{b_N} \frac{\sin^2(\omega - \phi)}{tg\gamma} \left(\sqrt{1 + \frac{tg^2\gamma}{\sin^2(\omega + \phi)}} - 1 \right) \quad \textbf{(16)}$$

$$P_{1-2-3-4} = \frac{h^*}{b_N} \ln\left(1 + \frac{h_N}{h^*}\right) \quad \textbf{(17)}$$

$$P_{1-4} = \frac{h_N^2}{2b_N \sin\gamma \left(h^* + \frac{h_N}{2}\right)} \quad \textbf{(18)}$$

$$P_{2-3} = \frac{h^* h_N}{b_N \sin\gamma \left(h^* + \frac{h_N}{2}\right)} \quad \textbf{(19)}$$

$$P_{3-7} = \frac{h^*}{h^* + h_N} \frac{f_{Na}}{f_{p-p}} \left(1 - \frac{2h_N}{b_N tg\gamma}\right) \quad \textbf{(20)}$$

$$P_{4-8} = \frac{h^*}{h^* + h_N} \left(1 + \frac{2h^*}{b_N} \left(\frac{1}{tg\gamma} - \frac{1}{\sin\gamma}\right) - \frac{2h_N}{b_N \sin\gamma}\right) \quad \textbf{(21)}$$

where h^* is the level of divergence of the grooves, γ is the angle of the deformation zone (Figure 7) and ω is the angle of the grooves, equal to arctan of A. P_{Ges} depends on γ and h^*. Then, it is necessary to minimize $P_{Ges}=f(\gamma, h^*)$ using a numerical minimization method. One possibility is to adopt the Rosenbrock algorithm [12], which is convenient for the optimization of functions with several variables.

The coefficient of friction acting on the area of the grooves (f_e) can be obtained from:

$$f_e = f_{p-p} P_{Ges\min} \quad \textbf{(22)}$$

Finally, the average effective friction coefficient is obtained by substituting f_{p-p} by f_e in expression 2:

$$f_{ef} = f_b + (f_e - f_b)\frac{B}{\pi D_b} \quad \textbf{(23)}$$

4- Effect of the geometry of the grooves

4.1- Geometry and polymer properties

The extruder to be used in the calculations has a square pitch screw with a diameter of 36 mm and a *L/D* ratio equal to 26. Sleeves 4D long (144 mm) containing grooves with different geometries can be exchanged. In all cases, the grooves have a maximum depth at the beginning, which decreases linearly downstream until cancelling out. Table 1 presents the various configurations used for the grooves.

Table 1- Geometry of the grooves tested.

Configuration	N_N	b_N (mm)	$N_N * b_N$ (mm)
1	12	5.0	60
2	10	6.0	60
3	8	7.5	60
4	6	10.0	60
5	4	15.0	60
6	12	4.0	48
7	12	6.0	72

The polymer used in the calculations is a High-Density Polyethylene, a thermoplastic typically used for pipes and blown film, with the friction properties shown in Table 2.

Table 2- Friction coefficients for HDPE.

Friction coefficient polymer- barrel	0.45
Friction coefficient polymer- screw	0.25
Internal friction coefficient	0.669

4.2- Results with the various calculation methods

The four calculation methods presented in the previous section were used to determine the value of the global friction coefficient, f_{ef}, for the groove geometries of Table 1. Figure 8 shows the effect of h_N/b_N on f_{ef} for configuration 1. As expected, the models of Goldacker and Rautenbach are insensitive to channel depth. In the case of the model of Potente, f_{ef} varies continuously; two regimes are present for the model of Grünschlo

β, i.e., when $h_N/b_N < 0.06$, f_{ef} takes one value, whereas for the remaining values of h_N/b_N the coefficient of friction is the same as that given by the Goldacker model. Indeed, both models use equations 2 and 23 when $P_{Ges\ mín}$ converges to 1.

Configurations 1 to 5 in Table 1 have different geometries at constant $N_N * b_N$. Figures 9 and 10 reveal that the models of Goldacker and Potente do not account for these changes. In the Rautenbach model (Figure 11), the effect of N_N does not follow a clear trend and when there are less than six grooves, f_{ef} is lower than f_b. The Grünschloβ model (Figure 12) shows little sensitivity to N_N

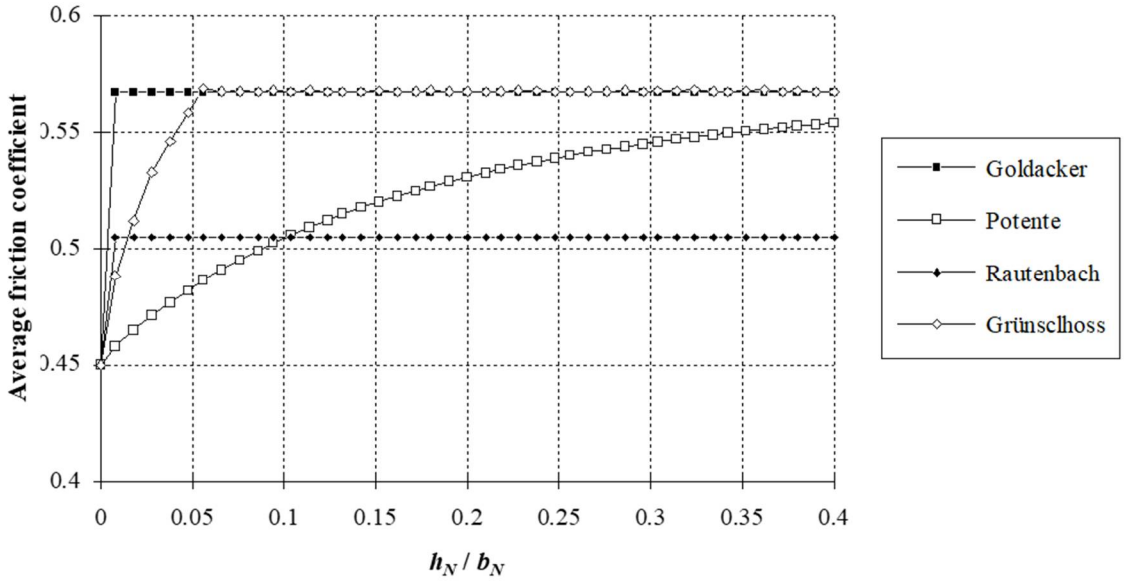

Figure 8- Effect of h_N/b_N on the average friction coefficient according to various calculation models.

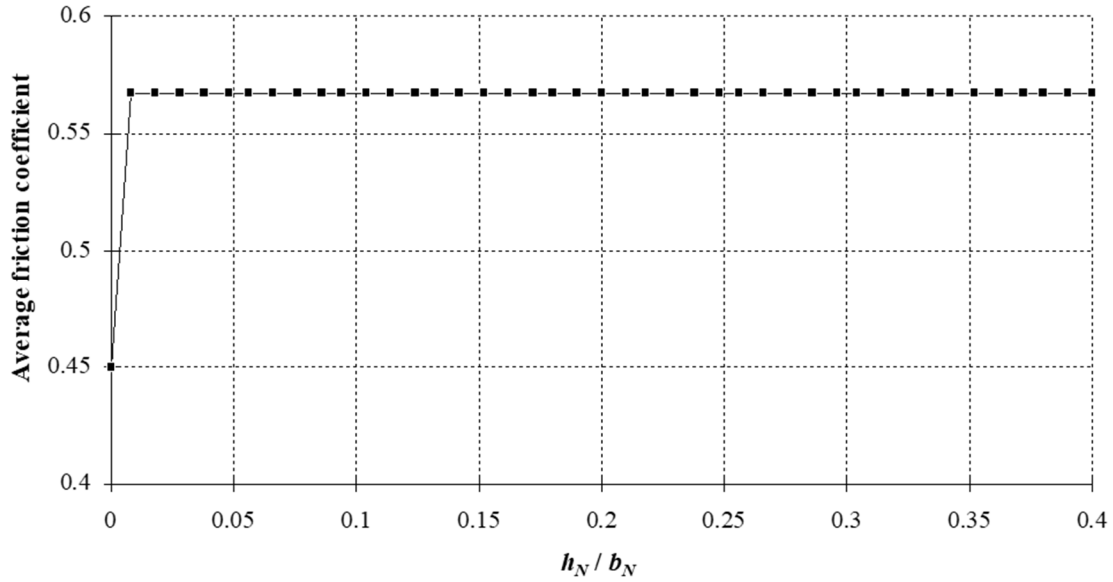

Figure 9- Average friction coefficient calculated by the Goldacker model (configurations 1 to 5).

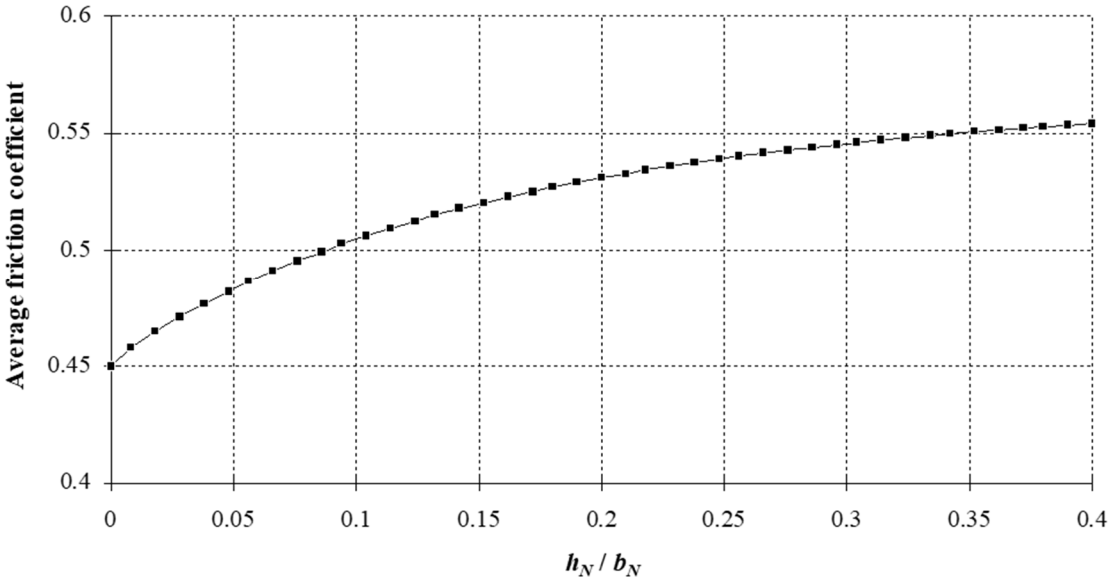

Figure 10- Average friction coefficient calculated by the Potente model (configurations 1 to 5).

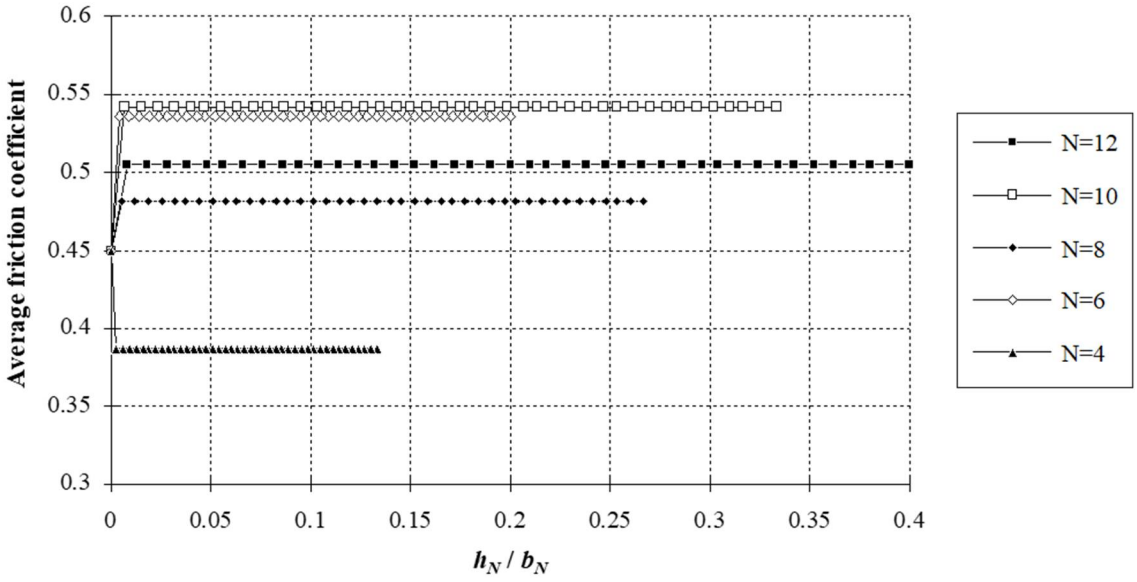

Figure 11- Average friction coefficient calculated by the Rautenbach model (configurations 1 to 5).

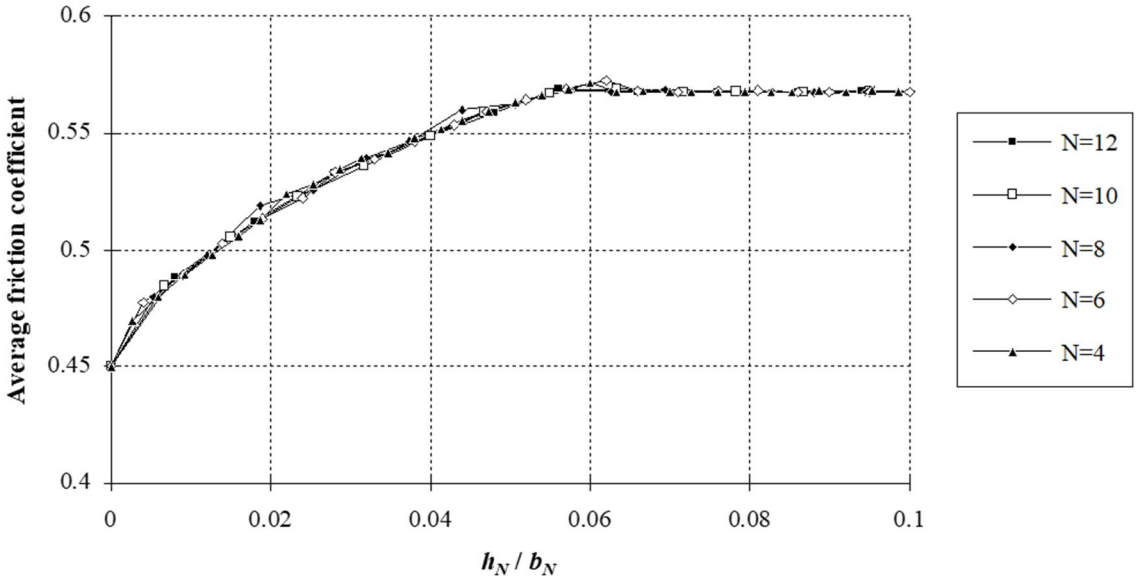

Figure 12- Average friction coefficient calculated by the Günschloβ model (configurations 1 to 5).

As seen in Figures 13 to 16, all the models are sensitive to variations in the total width of the grooves, B. Furthermore, a proportionality exists between both, as demonstrated in Table 3.

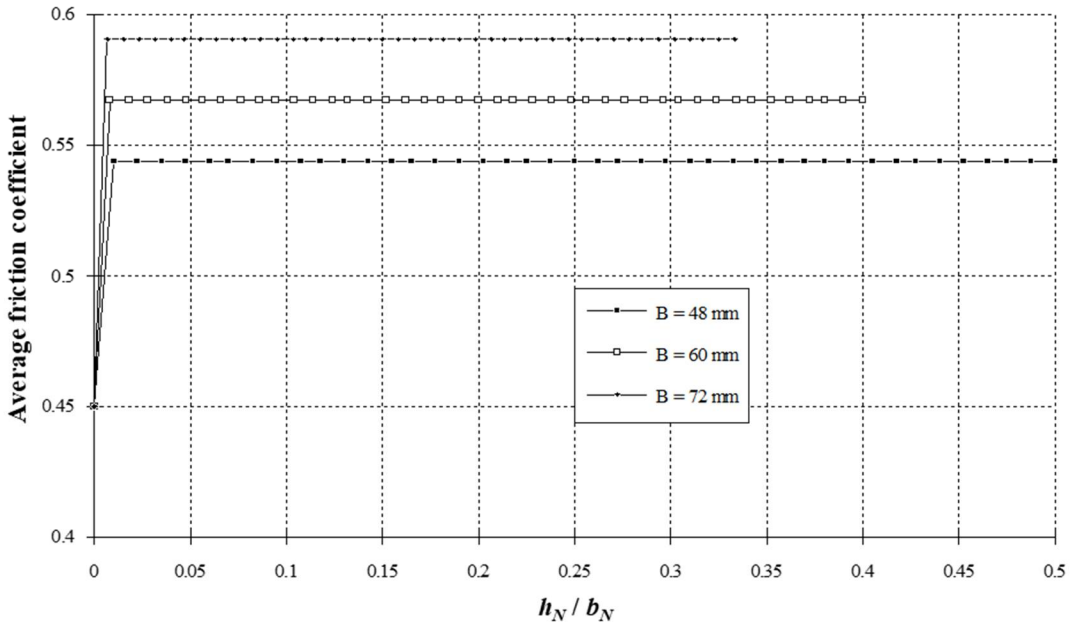

Figure 13- Effect of the total width of the grooves on the average friction coefficient (Goldacker model).

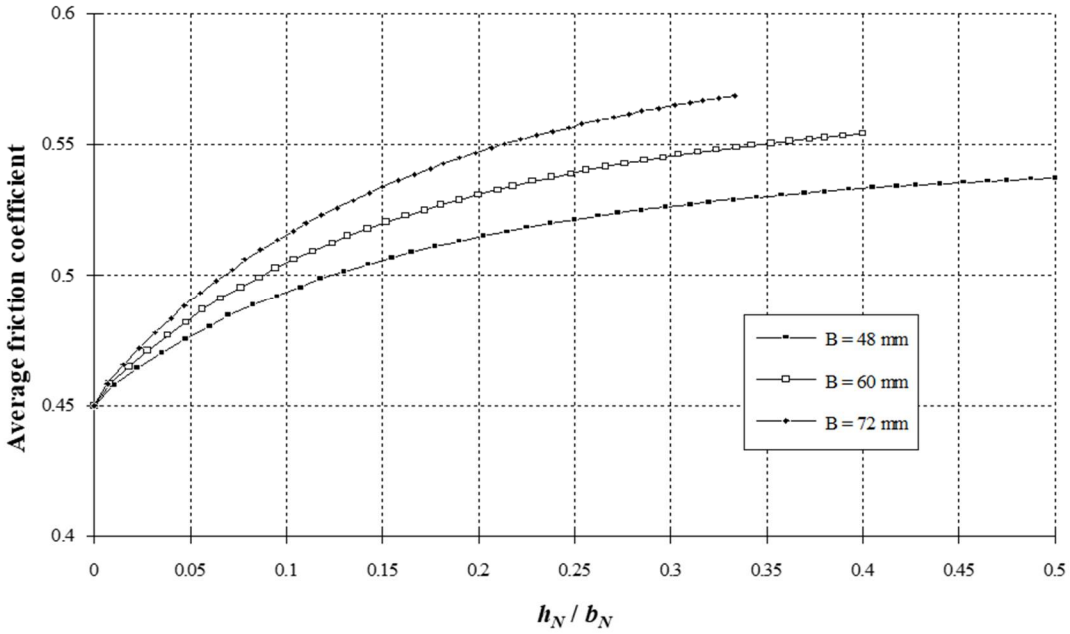

Figure 14- Effect of the total width of the grooves on the average friction coefficient (Potente model).

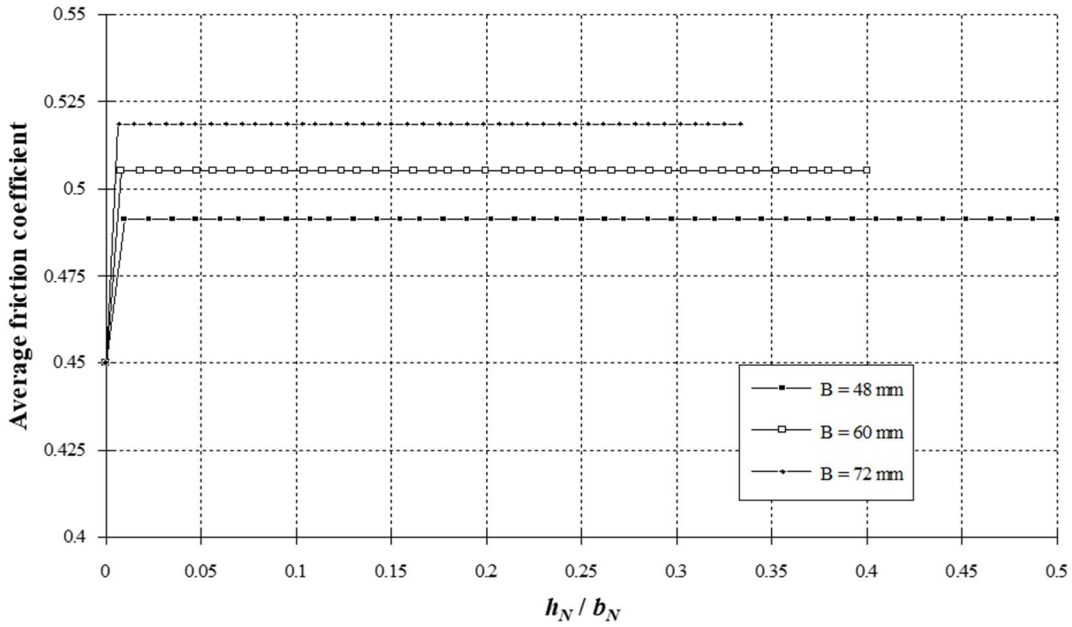

Figure 15- Effect of the total width of the grooves on the average friction coefficient (Rautenbach model).

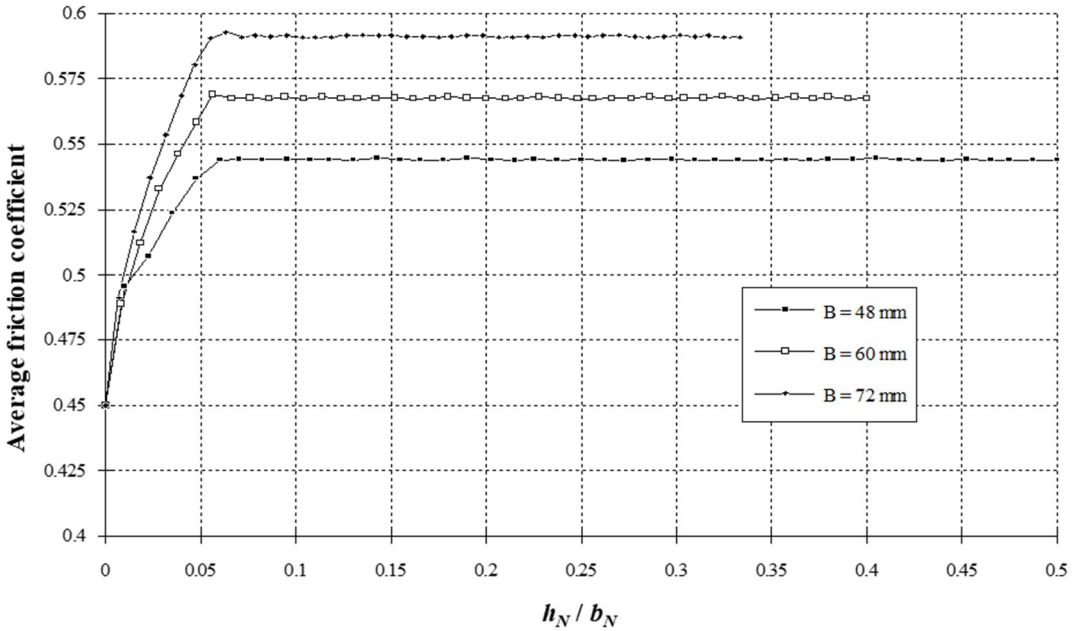

Figure 16- Effect of the total width of the grooves on the average friction coefficient (Grünschloβ model).

Table 3- Proportionality between f_{ef} and *B*.

Model	*B* (mm)	f_{ef} (máximo)
Goldacker	48/60/72	0.544/0.567/0.591
Potente	48/60/72	0.537/0.554/0.569
Rautenbach	48/60/72	0.491/0.505/0.519
*Grünschlo*β	48/60/72	0.544/0.568/0.591

Finally, Figure 17 shows the effect of the coefficient A^+ of the Rautenbach model on the value of f_{ef}. As shown, a variation of A^+ from 0.1 to 0.9 produces a change between 0.551 and 0.482 in f_{ef}.

Globally, these results show that the model of Potente is able to consider simultaneously the effect of the total width of the grooves (*B*) and of their depth (h_N), while remaining take in only the effect of one of these parameters.

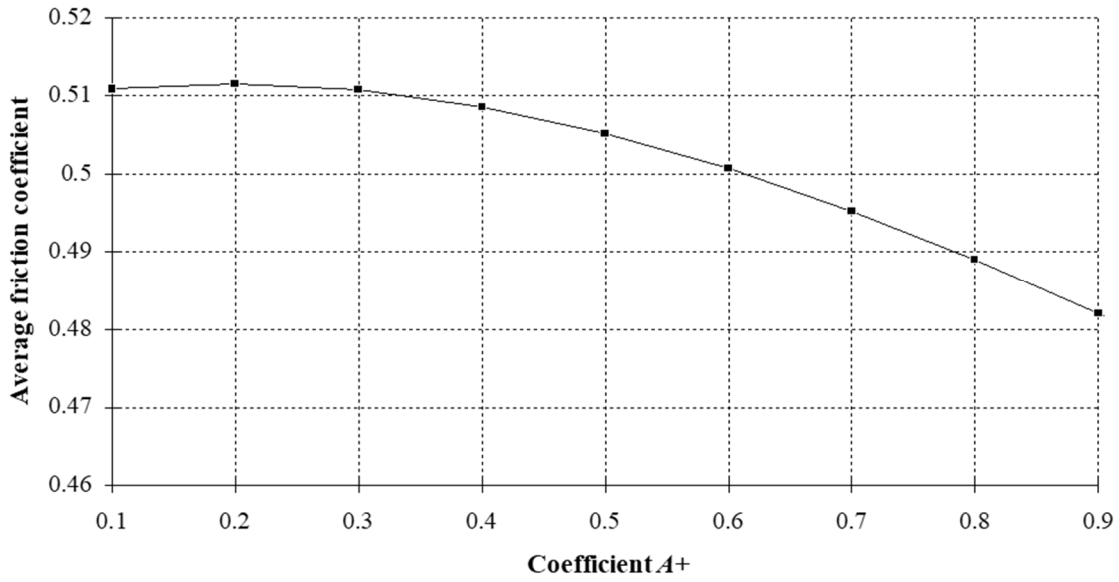

Figure 17- Influence of A^+ in the average friction coefficient.

4.3- Influence on plasticating extrusion

As discussed above, a higher friction coefficient between the polymer and the barrel will generate higher positive drag forces, hence higher pressure generation and higher output. Therefore, it is interesting to perceive what is the effect of the various methods to calculate f_{ef} on the predictions of a global modelling package of plasticating single screw extrusion (for details see the relevant chapter). The answer is given in

Table 4, which shows that the models that yield a higher effective friction coefficient (Goldacker and Grünschlo β) also induce a higher throughput.

Table 4- Predicted outputs when using different calculation methods for the effect of the grooves.

Calculation methods	Output (kg/hr)
Without grooves	8.06
Goldacker	8.32
Potente	8.07
Rautenbach	8.07
*Grünschlo*β	8.17

5- Application to a case study

This section uses one of the calculation methods above (the model of Potente), to study the effect of the geometry of the grooves on the performance of a laboratorial extruder. The aim is to generate data that later could be compared with values obtained experimentally.

5.1- Extruder, material and operating conditions

The layout of the extruder is represented in Figure 18. The three-zone screw has a diameter, D_{screw} = 25 mm, a L/D ratio of 25 and a square pitch. The lengths of the feed, compression and metering zones are 8D, 8D and 9D long, respectively. The internal screw diameter is 16.6 mm and 22.0 mm, respectively, in the feed, D_{i1}, and metering, D_{i3}, zones; the longitudinal length of the grooves, L_g, is 100 mm. A simple circular die is coupled at the end.

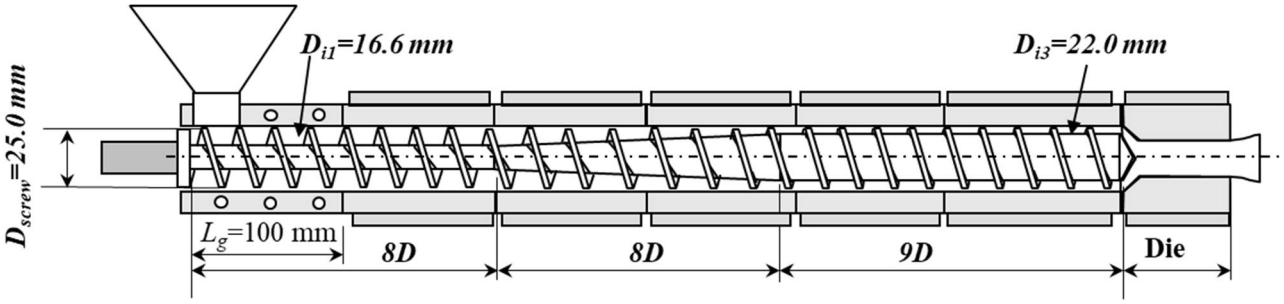

Figure 18- Extruder layout.

Table 5 shows the diverse geometries utilized. They could also correspond to different positions of devices allowing to adjust continuously the geometry of the grooves. In such a case, G1a represents the position when the grooves have the maximum value for the initial depth, h_{N0}, while G1d represents the case when this depth is nil.

Table 5- Geometry of the grooves studied.

Geometry	b_N (mm)	h_{N0} (mm)	N_N	L (mm)	$B = N_N * b_N$ (mm)
G1a	6.0	6.0	4	100.0	24
G1b	6.0	4.0	4	100.0	24
G1c	6.0	2.0	4	100.0	24
G1d	6.0	0.0	4	100.0	---
G1e	6.0	6.0	5	100.0	30
G1f	6.0	4.0	5	100.0	30
G1g	6.0	2.0	5	100.0	30
G1h	6.0	0.0	5	100.0	---

Table 6 presents the relevant properties of the polymer used, a Low-Density Polyethylene (grade Malen E FGAN 18-D003 produced by LyondellBasell). The melt viscosity (Figure 19) was measured by capillary rheometry, the data being fitted to a power law with an Arrhenius temperature dependence:

$$\eta = \eta_0 \, \gamma^{(n-1)} e^{-a(T-T_0)} \qquad \textbf{(24)}$$

Table 6- Main properties of LDPE (Basel Malen E FGAN 18-D003).

Properties			LDPE	Unity
Density	*Apparent*	ρ_0	495.0	kg/m^3
	Solid	ρ_s	921.0	kg/m^3
	Melt	ρ_m	854.4	kg/m^3
Friction coefficients	*Internal*		0.67	---
	Hopper		0.30	---
	Barrel		0.40	---
	Screw		0.20	---
Thermal conductivity	*Solid*	k_s	0.141	W/m ºC
	Melt	k_m	0.078	W/m·ºC
Specific Heat	*Solid*	C_s	3160.0	J/kg
	Melt	C_m	2682.0	J/kg
Melting heat		h	1.03 x 10^6	J/kg
Melting temperature		T_m	113.0	ºC
Viscosity: Power law with Arrhenius temperature dependence		n	0.27	---
		η_0	3.7e4	Pa/s
		a	0.005	1/°C
		T_0	170.0	°C

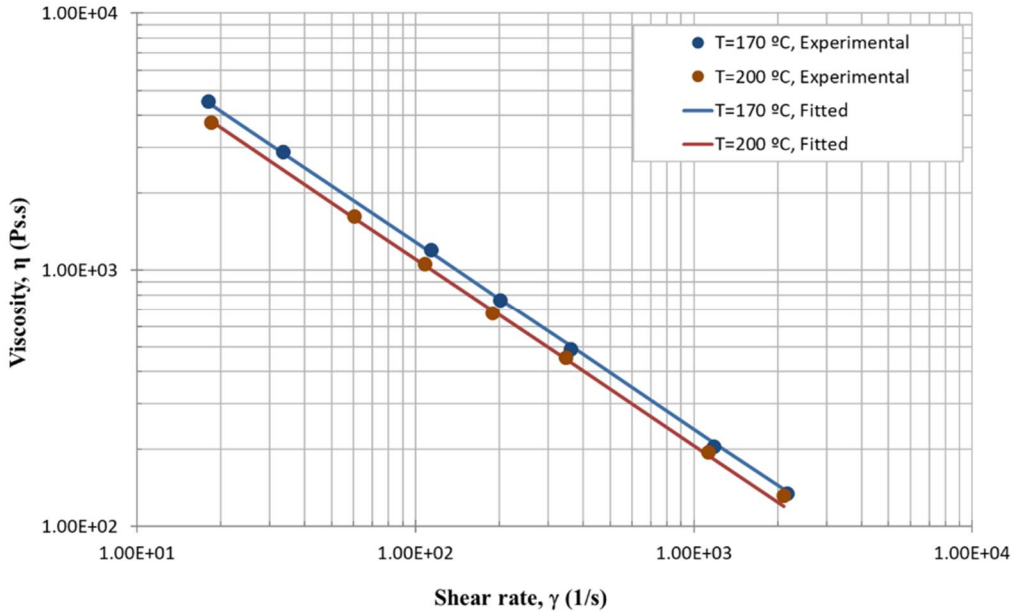

Figure 19- Rheological data for LDPE (Basel Malen E FGAN 18-D003).

In all calculations, the operating conditions were fixed. The screw speed was 120 rpm; the barrel set temperature profile during the first 5D (corresponding to the length of the grooves) varies linearly from 30 ºC and 70ºC in order to prevent melting of the polymer and is constant and equal to 170ºC in the remainder of the barrel and die.

4.2- Results

Figure 20 presents the axial development of pressure, *P*, solids width (*X/W,* where X is the width of the solids and W is the channel width), and maximum temperature in the solids, $T_{s\,max}$, together with the barrel temperature profile imposed, T_{Barrel}, for the geometry G1a. Table 7 shows the values of global extruder responses: output, average melt temperature at die exit, mechanical power consumption, length required for melting, degree of distributive mixing (quantified by *WATS*, a measure of the average total of the melt in the extruder [13]), and viscous dissipation (ratio between the maximum and the barrel temperatures). Observation of the temperature graphs in Figure 20 shows that $T_{s\,max}$ raises faster than T_{Barrel} due to the high rate of heat generated by friction. Consequently, the length of the solids conveying stage reduces and so does the pressure generation, which reaches only less than 9 MPa. As expected, the maximum pressure is attained near the end of the compression zone of the screw. Most of the melting stage develops along the compression zone and is completed before the metering zone.

The Potente model used to calculate f_{ef} is only sensitive to values of $h_N/b_N < 0.1$ (see Figure 14). For geometries G1a to G1c, B = 24, thus $h_N/b_N = 0.3$ at the beginning of the grooves ($h_{N0} = 2$); this ratio becomes

small only towards the end of the grooves, where the effect of f_{ef} on the pressure profile is minor. Therefore, the results for these three cases are very similar (Table 6).

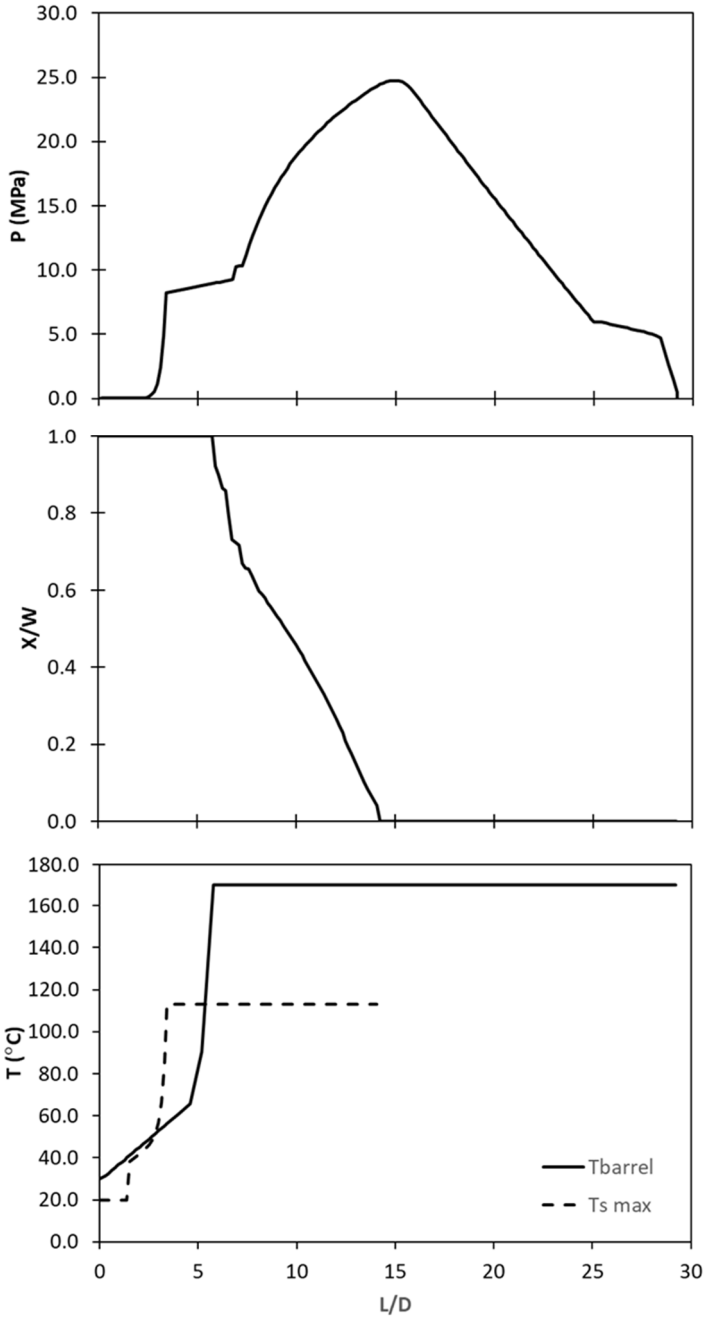

Figure 20- Results obtained when using grooves with the geometry G1a (Table 5).

Table 7- Results for the geometries G1 in Table 5.

Geometry	Output (kg/hr)	T_{melt} (°C)	Power consumption (W)	$L_{melting}$ (L/D)	*WATS*	Viscous Dissipation
G1a	5.43	188.5	2647	14.21	302.6	1.53
G1b	5.38	188.6	2597	14.17	303.1	1.54
G1c	5.38	188.6	2630	13.69	299.5	1.54
G1d	5.34	188.9	2278	14.64	308.0	1.46
G1e	5.47	188.3	2728	14.21	301.8	1.53
G1f	5.46	188.3	2669	13.83	299.2	1.51
G1g	5.35	188.3	2709	13.88	301.2	1.53
G1h	5.34	188.9	2278	14.64	308.0	1.46

Geometry G1e exhibits grooves with bigger depth and total width. As seen in Figure 21, the pressure can reach approximately 10 MPa, as expected. Conversely, G1d and G1h, where grooves are absent, are capable of inducing lower pressures than the remaining (Figure 22). As demonstrated in Figure 23, the various groove geometries will induce distinct pressure generations. Values between 6 MPa and 10 MPa will be obtained at the end of solids conveying. In turn, they will influence the remaining thermomechanical history of the material in the extruder, yielding the differences summarized in Table 7.

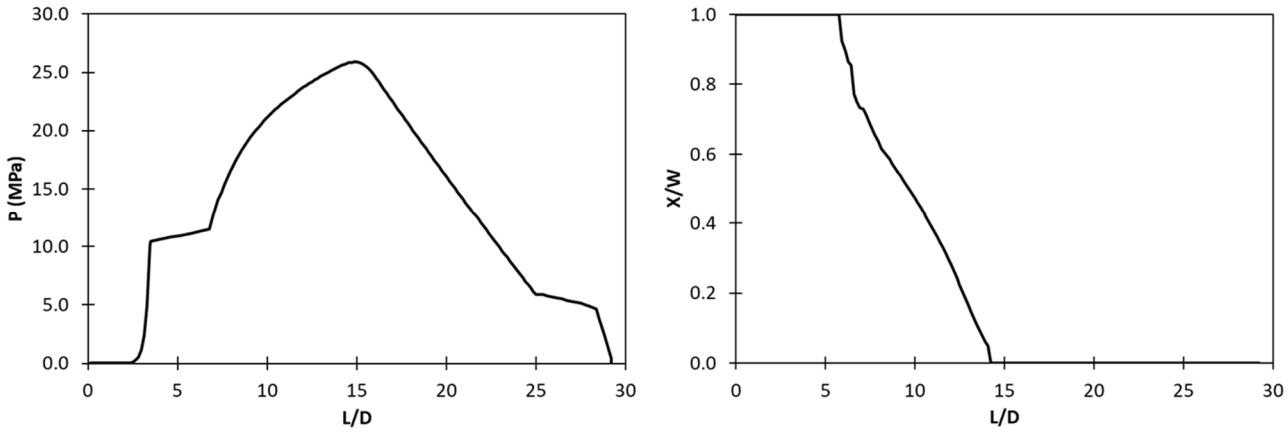

Figure 21- Results obtained when using grooves with the geometry G1e (Table 5).

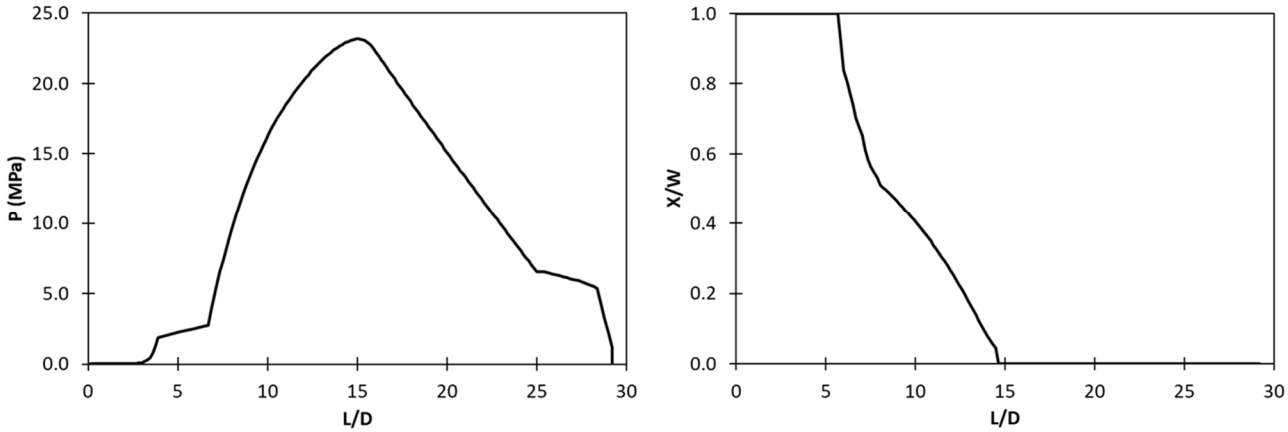

Figure 22- Results obtained when using grooves with the geometries G1d and G1h (Table 5).

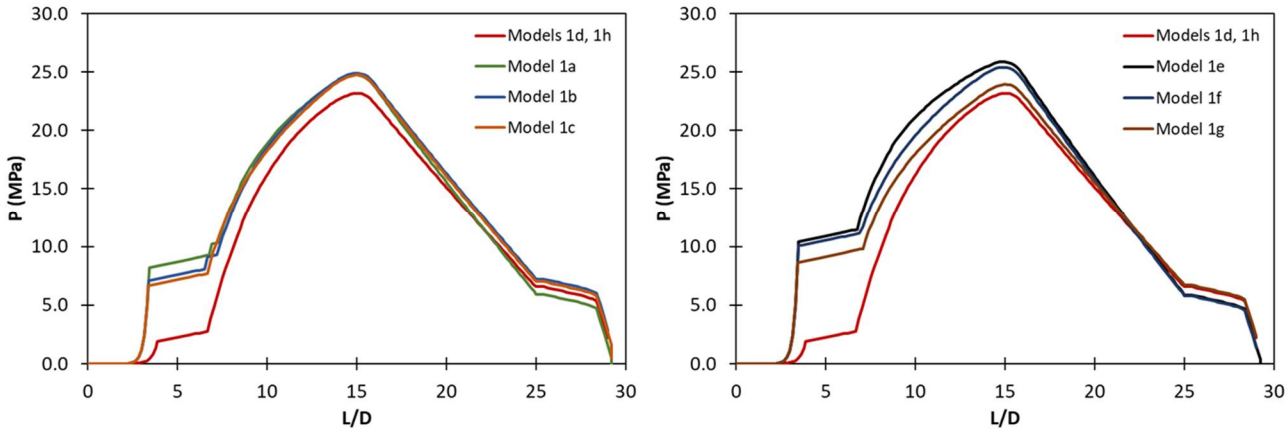

Figure 23- Pressure profiles for the geometries G1 (in Table 6).

6- Conclusions

The presence of grooves in the initial part of the barrel can affect significantly the performance of single screw extruders. Modelling their effect would enable the development of suitable and reliable process modelling routines. One possible approach is to calculate the global friction coefficient between barrel and polymer, f_{ef}, that is created by the presence of the grooves. The more sensitive f_{ef} would be to the geometrical parameters of the grooves, the better. This chapter assessed the suitability of four calculation methods of f_{ef}. It was shown that the equation developed by Potente considers both the width and depth of the grooves, whilst the model of Goldaker has the strongest influence on the plasticating sequence.

The examples discussed showed that the presence of the grooves does indeed improve the performance of the extruder in terms of pressure generation and output, but their geometry, particularly depth and the total width, greatly influences the behaviour.

7- References

[1] H. Darnell, E.A.J. Mol, SPE J., **12**, 20, 1956

[2] Tadmor, Z.; Klein, I., "Engineering Principles of Plasticating Extrusion", Van Nostrand Reinhold, Ney York, 1970

[3] Rawendaal, C., "Polymer Extrusion", Hanser Publishers, Munich, 1986

[4] Boes, D.; Krämer, A.; Lohrbäccher, V.; Scheneiders, A., Kunststoffe Germ. Plast., **80**, 6, 659, 1990

[5] Potente, H., Kunststoffe Germ. Plast., **75**, 7, 439, 1985

[6] Rautenbach, R., Peiffer, H., Kunststoffe Germ. Plast., **72**, 3, 137, 1982

[7] Rautenbach, R., Peiffer, H., Kunststoffe Germ. Plast., **72**, 5, 262, 1982

[8] Grünschloss, E., Kunsttoffe Germ. Plast., **74**, 7, 405, 1984

[9] Potente, H., Kunststoffe Germ. Plast., **78**, 4, 355, 1988

[10] Potente, H., Koch, M., Intern. Polym. Process., **4**, 4, 288, 1989

[11] Goldacker, E., Diss. RWTH Aachen, 1971

[12] Rosenbrock, H.H., The Computer Journal, **3** , 3, 175, 1960

[13] G. Pinto, Z. Tadmor, Polym. Eng. Sci., **10**, 279, 1970